

COMMON ENVELOPE EJECTION FOR A LUMINOUS RED NOVA IN M101

N. BLAGORODNOVA ¹, R. KOTAK ², J. POLSHAW ², M. M. KASLIWAL ¹, Y. CAO ¹, A. M. CODY ⁷, G. B. DORAN ⁹,
 N. ELIAS-ROSA ⁸, M. FRASER ³, C. FREMLING ⁴, C. GONZALEZ-FERNANDEZ ³, J. HARMANEN ¹¹, J. JENCSOON ¹,
 E. KANKARE ², R.-P. KUDRITZKI ¹², S. R. KULKARNI ¹, E. MAGNIER ¹², I. MANULIS ⁵, F. J. MASCI ¹, S. MATTILA ^{3,11},
 P. NUGENT ⁶, P. OCHNER ⁸, A. PASTORELLO ⁸, T. REYNOLDS ^{11,13}, K. SMITH ², J. SOLLERMAN ⁴, F. TADDIA ⁴,
 G. TERRERAN ^{2,8}, L. TOMASELLA ⁸, M. TURATTO ⁸, P. VREESWIJK ⁵, P. WOZNIAK ¹⁰, S. ZAGGIA ⁸

Draft version April 24, 2022

ABSTRACT

We present the results of optical, near-infrared, and mid-infrared observations of M101 OT2015-1 (PSN J14021678+5426205), a luminous red nova in M101 galaxy, spanning 16 years. The lightcurve of the object showed two peaks with absolute magnitudes $M_R \leq -12.4$ and $M_R = -12$, on 2014 November 11 and 2016 February 17 respectively. The spectral energy distributions during the second maximum show a cool outburst temperature of ≈ 3700 K and low velocity (≈ 300 km s⁻¹) for H I, Ca II, Ba II and K I lines. Archival data, from 15 to 8 years before the outburst, show a progenitor star that is an F-type yellow super-giant with $L \geq 8.7 \times 10^4 L_\odot$ and temperature ≈ 7000 K. This star has just finished the H burning phase in the core, started expanding, and now is crossing the Hertzsprung gap. We argue that the progenitor is a binary system, with masses $M1 \sim 18 M_\odot$ and $M2 \sim 16.2 M_\odot$, with the more evolved system overfilling the Roche lobe. Comparison with binary evolution models supports the hypothesis that the outburst was an extremely rare phenomena, likely associated with the the ejection of the common envelope. The initial masses of the binary progenitor system, fills the gap between the merger candidates V 838 Mon ($5-10 M_\odot$) and NGC 4490-OT ($30 M_\odot$).

Subject headings: binaries: close – stars: peculiar – stars: novae –stars: individual (M101 OT2015-1, PSN J14021678+5426205, iPTF13afz), stars: massive, binaries (including multiple): close, stars: winds, outflows

1. INTRODUCTION

The discovery of an unusually bright and red nova in M31 (M31 RV) in September 1988, triggered the initial attention of astronomers (Rich et al. 1989) towards an uncommon type of objects. Its peak luminosity, $M_V = -9.95$, was brighter than a regular nova ($M_V = -6$ to -8), but fainter than a Supernova ($M_V < -14$ mag). The unusually cool temperature, similar to an M0 type super-giant, and high ejected mass, placed the object into a potentially different category from known cataclysmic

variables eruptions, triggering the need for further theoretical exploration. Since then, transient surveys and discoveries led by amateurs contributed to further populate this luminosity “gap” between classical novae and supernovae (SNe) (Kasliwal et al. 2011). As of today, the observational diversity of such intermediate luminosity events on long timescales (>20 days) encompasses three main categories: SN impostors, originated by eruptions in massive stars, such as luminous blue variables (LBV), intermediate luminosity optical (red) transients (ILOT/ILRT), explained as terminal faint explosions and luminous red novae (LRNe), which are potential stellar mergers.

Luminous non-terminal outbursts of massive stars sometimes may mimic the observational signature of a SN. Consequently, this class of event was named as “SN impostors”. Among these, eruptions of LBV are known to produce intermediate luminosity transients (Humphreys & Davidson 1994), such as Eta Carinae and P Cygni. These classical examples generally inhabit the upper part of the Hertzsprung-Russell (HR) diagram, having bolometric magnitudes greater than $M_{Bol} = -9.5$ mag, in the super-giant region. Generally, LBV progenitors exhibit giant eruptions with visual changes >2 mag, but also they show non-periodic variability consistent with the behaviour of known LBVs in the LMC: R127 and S Doradus (Wolf 1989; Walborn et al. 2008, and references therein). As a consequence, the progenitor stars are generally living in a dusty environment, caused by previous episodes of mass ejections. The non-terminal eruptions of SN 2009ip (Pastorello et al. 2013; Mauerhan et al. 2013; Fraser et al. 2013) and UGC 2773 OT2009-1 (Foley et al. 2011; Smith et al. 2016a) are examples of

¹ Cahill Center for Astrophysics, California Institute of Technology, Pasadena, CA 91125, USA

² Astrophysics Research Centre, School of Mathematics and Physics, Queen’s University Belfast, Belfast BT7 1NN, UK

³ Institute of Astronomy, University of Cambridge, Madingley Road, CB3 0HA, Cambridge, UK

⁴ Department of Astronomy, The Oskar Klein Center, Stockholm University, AlbaNova, 10691 Stockholm, Sweden

⁵ Department of Particle Physics and Astrophysics, Weizmann Institute of Science, Rehovot 7610001, Israel

⁶ Lawrence Berkeley National Laboratory, Berkeley, California 94720, USA

⁷ Spitzer Science Center, California Institute of Technology, 1200 East California Boulevard, Pasadena, Ca 91125, USA

⁸ INAF-Osservatorio Astronomico di Padova, Vicolo dell’Osservatorio 5, I-35122 Padova, Italy

⁹ Jet Propulsion Laboratory, California Institute of Technology, Pasadena, CA 91125, USA

¹⁰ Los Alamos National Laboratory, MS-D466, Los Alamos, NM 87545, USA

¹¹ Tuorla Observatory, Department of Physics and Astronomy, University of Turku, Väisäläntie 20, FI-21500 Piikkiö, Finland

¹² Institute for Astronomy, University of Hawaii, 2680 Woodlawn Drive, Honolulu, HI 96822, USA

¹³ Nordic Optical Telescope, Apartado 474, E-38700 Santa Cruz de La Palma, Spain

LBV in their cool eruptive phase.

ILRT, such as SN 2008S (Prieto et al. 2008; Botticella et al. 2009; Thompson et al. 2009), NGC 300 2009OT-1 (Bond et al. 2009; Smith et al. 2011) and iPTF10fqs (Kasliwal et al. 2011) dominate the luminous part of the “gap” transient family (Kasliwal 2011). Such events have been interpreted as faint terminal explosions associated to dusty progenitors (Prieto et al. 2008, 2009; Kochanek 2011). The electron-capture SNe scenario has been suggested as a possible mechanism (Botticella et al. 2009). Late time observations reveal the complete disappearance of their progenitors, suggesting their outburst to be a terminal activity (Adams & Kochanek 2015). A survey of massive stars in M33 revealed that the rate of SN 2008S and the NGC 300-OT-like transient events was of the order of $\sim 20\%$ of the CCSN rate in star-forming galaxies in the local Universe ($D_L \lesssim 10$ Mpc) (Thompson et al. 2009). However, the fraction of massive stars with colours similar to the progenitors of these transients was only $\lesssim 10^{-4}$. Khan et al. (2010) showed that similar stars were as rare as one per galaxy. The direct implication is that the heavy dust environment phase is a very short transition phase for many massive stars during their last 10^4 years.

Violent binary interactions in binary systems (including stellar mergers) were suggested as the plausible scenario to explain the nature of the outbursts of LRNe (Iben & Tutukov 1992; Tylenda et al. 2011; Nandez et al. 2014). Nova Scorpii 2008 (V1309 Sco) currently provides the most compelling evidence for a merger scenario in our own Galaxy, as the exponential period decay of the progenitor system could be witnessed from observations spanning several years before the outburst (Mason et al. 2010; Tylenda et al. 2011, 2013; Nandez et al. 2014). V833 Mon, at 6.1 ± 0.6 kpc (Sparks et al. 2008) is another remarkable example of a stellar merger scenario, including a spectacular light echo, revealed by observations with the Hubble Space Telescope (Bond et al. 2003). Some extragalactic examples of discoveries consistent with the merger scenario are M85-OT2006OT-1¹⁴, the luminous red nova in M31, reported in Williams et al. (2015) and the massive stellar merger NGC 4490 2011OT-1 (Smith et al. 2016b). Pre-explosion photometry of the progenitor systems has allowed to estimate the mass and evolutionary stage of the progenitor system. To date, literature reports a wide range of cases, from 1.5 ± 0.5 M_\odot for V1309 Sco to $20-30$ M_\odot for NGC 4490 2011OT-1 Smith et al. (2016b).

In this work, we will discuss the observations and nature of M101 OT2015-1 (hereafter M101-OT), also designated as PSN J14021678+5426205 and iPTF13afz, an extragalactic transient in the luminosity gap. The discovery of M101-OT was publicly announced on CBAT by Dimitriu Cipriani Vintdevara on the night of 10th to 11th of February 2015 in the outskirts of NGC 5457 (M101)¹⁵. Shortly after it was confirmed as an optical

¹⁴ Although M85 2006OT-1 is observationally similar to other LRNe, the interpretation of its nature is more controversial. Kulkarni et al. (2007) (see also Ofek et al. (2008), Rau et al. (2008)) supported the idea of a low-to-moderate mass merger, while Pastorello et al. (2007) favoured the weak core-collapse SN explosion scenario.

¹⁵ <http://www.cbat.eps.harvard.edu/unconf/followups/J14021678+5426205.html>

transient by Stu Parker with an unfiltered magnitude of 16.7. The source also had an independent discovery within the iPTF survey back in 2013, when it was identified as a slow rising source. In this paper, we investigate the observational signature and the progenitor scenario for M101-OT. In Section 2, we report both pre- and post-discovery optical, near-infrared (NIR) and mid-infrared (MIR) photometry and spectroscopy of M101-OT. In Section 3, we examine the characteristics of the progenitor and the spectroscopic measurements. We discuss possible relations with similar objects and the nature of M101-OT in Section 4. Finally, we present a summary and our conclusions in Section 5.

2. OBSERVATIONS

M101-OT is located ($\alpha_{J2000} = 14^{\text{h}}02^{\text{m}}16^{\text{s}}.78$ $\delta_{J2000} = +54^{\circ}26^{\prime}20^{\prime\prime}.8$) in the outer reaches of a spiral arm of M101, at $3^\circ.41$ N and $8^\circ.12$ W of the measured position of the galaxy nucleus. The surrounding region shows signs of a young stellar population, displaying bright unresolved emission in the Galaxy Evolution Explorer (GALEX) survey at 135 nm to 280 nm.

We adopt the Cepheid distance to M101 of $D_L = 6.4 \pm 0.2$ Mpc, corresponding to a distance modulus of $\mu = 29.04 \pm 0.05$ (random) ± 0.18 (systematic) mag (Shappee & Stanek 2011). The estimated Galactic reddening at the position of the transient is $E(B-V) = 0.008 \pm 0.001$ mag (Schlafly & Finkbeiner 2011), with $R_V = 3.1$, which corresponds to a mean visual extinction of $A_V = 0.024$ mag. The magnitudes reported here are corrected for Galactic reddening. The exception are the magnitudes reported in the Appendices, which report the observed measurements. The extinction within the host galaxy is not included. However, archival NIR images do not show evidence of dust emission component in the progenitor star.

2.1. Photometry

The location of M101-OT has been serendipitously imaged by numerous telescopes and instruments over the last 15 years (from 2000 to 2015). In 2011, the galaxy became a special focus of attention, as it hosted one of the youngest SN Ia discovered so far: SN 2011fe (Nugent et al. 2011). We retrieved all available data covering the location of the transient in an attempt to piece together its previous evolution. Through this work, we will use the epoch of the second peak in r -band, MJD 57070.

Our best quality pre-discovery image (seeing of $0''.55$) was an r -band exposure at -3625 days from the Canada France Hawaii Telescope (CFHT). We aligned this image with our $+22$ -d post-peak image using 18 stars in common. There is one point source (see right hand side of Figure 1) in the image within a $2''$ radius of the position during the outburst, and the central position of the point spread functions (PSFs) are coincident within 180 mas. We identify this point source as the progenitor of M101-OT. Imaging in I -band taken at late times with Keck confirm the disappearance of the progenitor star.

Figure 1 shows the location of M101-OT for -10 yr, -1.8 yr and an early follow-up epoch at 22 days after the second peak. The system has faded below detectable limits at $+383$ days.

The historical optical data for M101-OT was retrieved

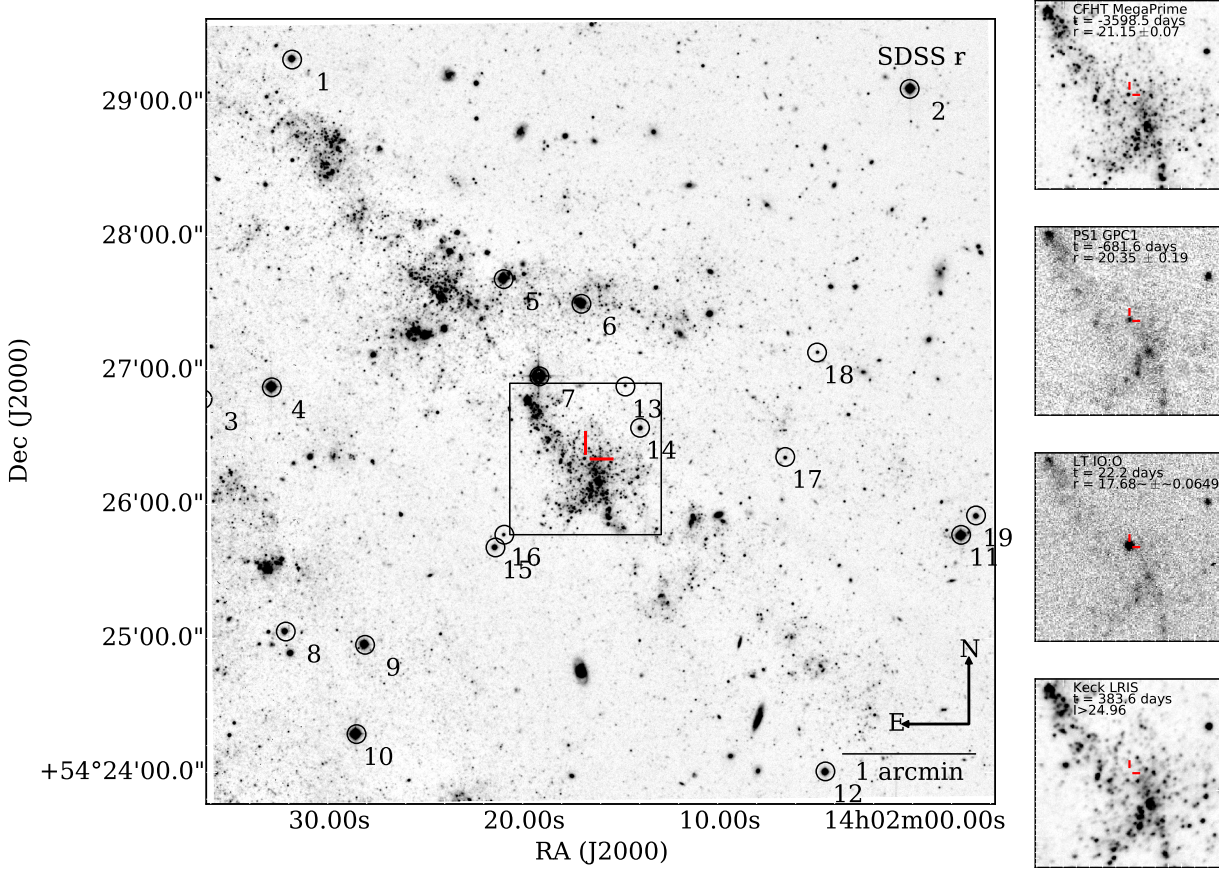


FIG. 1.— Left: M101-OT and the sequence stars used to calibrate the photometric zero-point. Due to a variable field-of-view, position and position angle for the M101-OT historical photometric images, different subsets of the field stars were used according to their visibility. At any time, a minimum number of three stars was used. The square region around M101-OT is shown in detail on the right hand side. The field is cut on the left side because of the limited coverage of the image. Right: Images of M101-OT at four epochs: ≈ 10 yrs before reference epoch, 22.3 month, 22 days after the second outburst and 12.6 months after. The field of view size is $1' \times 1'$ centred on the position of M101-OT. The red dashes show the location of the transient. The telescope, instrument, and magnitude of the object are listed for each image.

from the CFHT MegaPrime and CFHT12K/Mosaic, using single and combined exposures (Gwyn 2008), Pan-STARRS-1/GPC1 (Magnier et al. 2013; Schlaflay et al. 2012; Tonry et al. 2012, PS1);, INT/WFC and Sloan Digital Sky Survey (SDSS) DR 10 (Ahn et al. 2014). Post discovery magnitudes were obtained from the reported follow-up ATels, Liverpool Telescope (LT), the Nordic Optical Telescope (NOT) and the Palomar P48 and P60 telescopes. Details of pre-discovery photometry and post-discovery optical photometry may be found in the Appendices Table 1 and Table 2 respectively. PTF photometry is reported in Table 3. The infrared data were retrieved from CFHT/WIRCam, UKIRT/WFCAM and the Spitzer Infrared Array Camera (Fazio et al. 2004) in 3.6 and 4.5 μm . The NIR and MIR observations are summarized in Appendix Table 4.

We measured the brightness of the source coincident with M101-OT using the IRAF (Image Reduction and Analysis Facility) SNOoPY¹⁶ package for PSF photometry. The zero-point in the SDSS photometric system was calibrated using aperture photometry on three to nineteen different sequence stars in the M101-OT field.

Figure 1 shows the position of the sequence stars. Their coordinates and magnitudes are reported in Table 5. The magnitude measurements for bands *grizy* were obtained from the PS1 catalogue, having photometric accuracy better than 0.01 mag. Measurements for *u*-band were obtained from the SDSS DR10 catalogue. Johnson photometry was calibrated using the same PS1 catalogue and transformations provided by Tonry et al. (2012) with an RMS below 0.1 mag. Photometry from the PTF survey was obtained with the PTF Image Differencing Extraction (PTFIDE) pipeline for the 48-inch telescope (Masci et al. 2014) and with a custom difference imaging pipeline for 60-inch telescope at Mount Palomar (Cenko et al. 2006). Transformations from PTF Mould-*R* and *g*-band to SDSS equivalent photometry were obtained using the transformations in Ofek et al. (2012). The NOT NIR reductions were based on using an external IRAF package NOTCAM VERSION 2.5¹⁷ and a custom pipeline for WIRC data. The zero-point for IR photometry was calibrated using the Two Micron All Sky Survey (2MASS) photometry.

The full historical lightcurve of M101-OT is shown in Figure 2, left panel. The earliest detection of the pro-

¹⁶ SNOoPY is a package developed by E. Cappellaro, based on DAOPHOT, but optimized for SN magnitude measurements.

¹⁷ <http://www.not.iac.es/instruments/notcam/guide/observe.html>

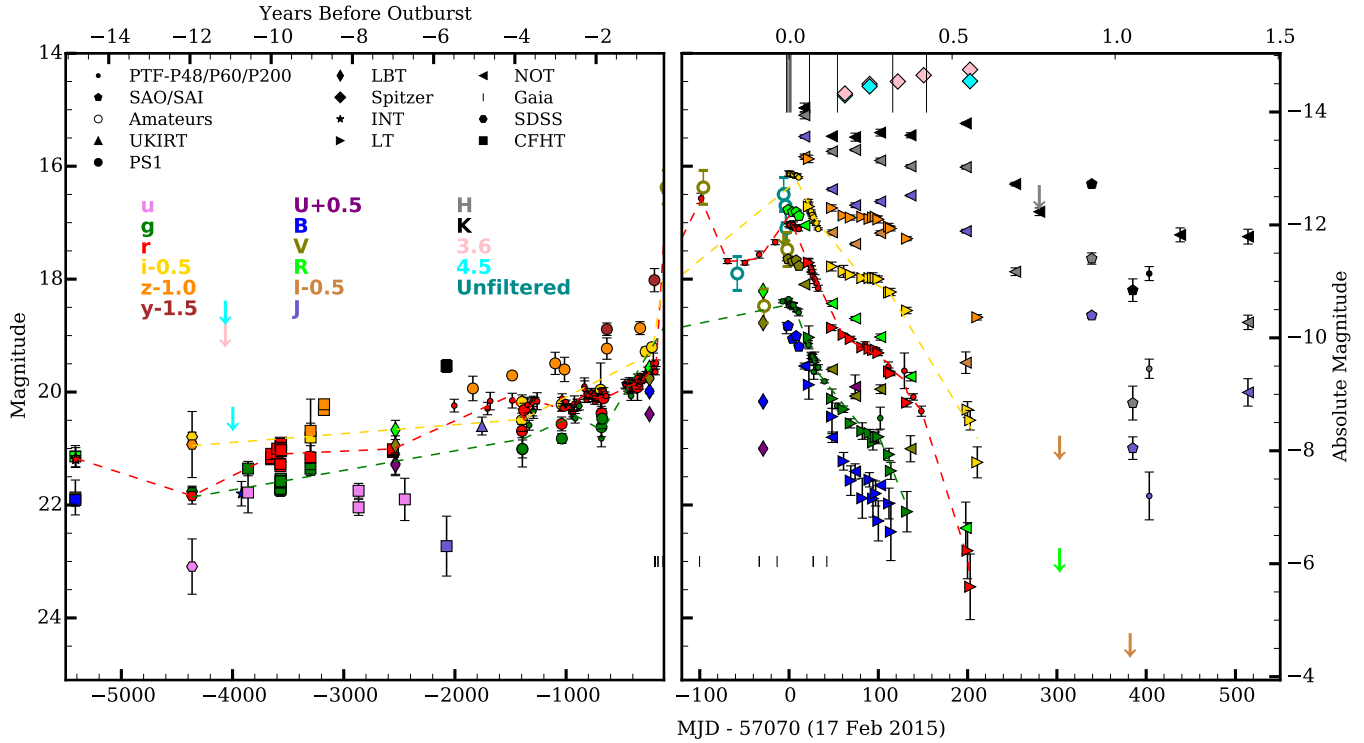


FIG. 2.— Left: Historic light curve for M101-OT spanning fifteen years of observations until 120 days before second peak date. Pan-STARRS1 and PTF data allow us to notice an increase in the baseline magnitude of the transient at about 5.5 years before the eruption. Dashed lines are used to guide the eye. Downward-pointing arrows indicate upper limits. Right: Close up of the lightcurve from -120 days to $+550$ days after outburst. For each data point, the marker shape shows the telescope and the colour indicates the filter. Note the difference in time scale between the left and right hand side plots. Vertical tickmarks below the lightcurve show the epochs when this object was observed by *Gaia* (yet non-public data). Upper vertical lines show the epochs when spectra were taken. The lightcurve shows two maxima at ~ -100 and 0 days.

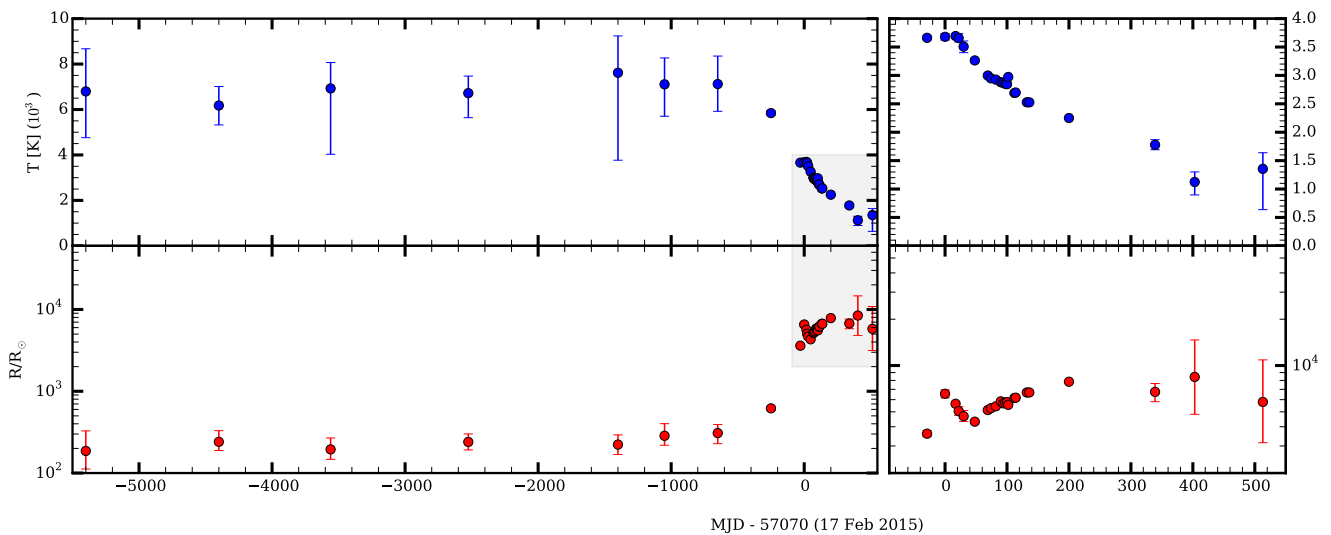


FIG. 3.— Left: Best fit for black-body temperature and radius evolution for M101-OT derived from photometry fits for the same time span as the lightcurve. We refer to the analysis in Section 3. Right: Zoom from -90 to $+550$ days corresponding to the region shaded in light grey in the left panel.

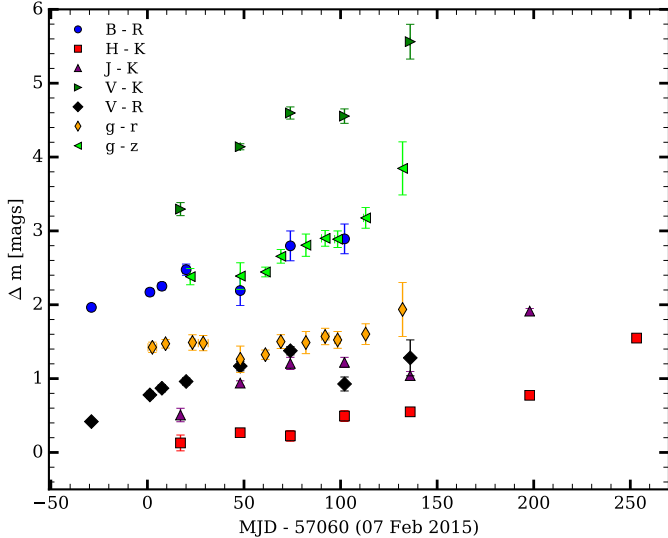


FIG. 4.— Post-outburst colour evolution for M101-OT. The data points have been binned in groups of 10 days. The abscissa is the average MJD of the bin relative to the reference epoch.

genitor was obtained on 2000 February 05 (all dates in this convention) with CFHT. From these observations, we get $B = 21.9 \pm 0.1$, $V = 21.8 \pm 0.3$, $R = 21.1 \pm 0.2$ (corrected for Milky Way reddening), which at the distance of M101 yield an absolute magnitudes of $M_B = -7.1$, $M_V = -7.2$, and $M_R = -7.9$ for the progenitor star. INT observations in the r -band, $r = 21.2 \pm 0.15$, taken only three days after CFHT, are consistent within 0.1 mag with the R -band measurements.

Within the first period, from approximately 15 to 5.5 years before outburst, the brightness of the progenitor shows only minor variations. The magnitude in the r -band remained constant to within 0.2 mags, with an average value of $r = 21.1$. Roughly 5.5 years before the outburst, the lightcurve began to rise smoothly across all bands. The r -band increased to 19.6 mag at -180 days i.e. 1.5 mag regarding the historical median value. Reported magnitudes prior to mid-2012 (-2.7 years) taken with the Large Binocular Telescope (LBT) agree with these values: the source was reported as being variable, with mean magnitudes of $U = 21.33 \pm 0.19$, $B = 21.30 \pm 0.19$, $V = 20.97 \pm 0.17$, and $R = 20.69 \pm 0.17$ (Gerke et al. 2015). During its slow rise, the transient was internally detected on 4th of April 2013 (-684 days) by the Intermediate Palomar Transient Factory (iPTF) as a slowly brightening source.

On 2014 November 10, after appearing from behind the Sun, it was detected at 16.6 mag in R-band during its first outburst (Cao et al. 2015), ~ 3 months prior to public discovery. At approximately -29 days to peak, it was also detected by LBT in between the first and second outbursts at a considerably fainter magnitude of $R = 18.22 \pm 0.02$ (Gerke et al. 2015). At the time of public announcement on 2015 February 10, the object was close to its second peak, estimated to fall 10 days later, on 2015 February 17 (MJD 57070).

The Gaia satellite (Perryman et al. 2001) (a European Space Agency mission) serendipitously observed the region containing M101-OT during the time of the first peak. Unfortunately, these data have not been made

available to us. Due to this handicap in constraining the time of the first peak, we choose to adopt the epoch of maximum brightness of the second peak, at MJD 57070, as our reference epoch.

The follow-up photometry for M101-OT is shown in the right panel of Figure 2. The most remarkable feature of the lightcurve is the existence of two maxima. The object was observed during the decay phase of the first peak, having an absolute magnitude of $M_r \geq -12.6$ mag (we only have data on the decline part for the first peak, so the outburst could have been brighter). The second maximum, ~ 100 days after shows $M_r \simeq -12.0$ mag and it is followed by a fast declining phase, lasting ~ 50 days, when the object fades 2 magnitudes in r -band. The lightcurve makes a transition into a plateau phase of ~ 60 days: the redder riz -bands flatten, while the bluer Bg -bands continue to decline. After the end of the “plateau”, the transient resumes the initial decline rate in r -band. The first NIR follow-up data show magnitudes of $J = 15.45 \pm 0.3$, $H = 15.07 \pm 0.06$ and $K = 14.94 \pm 0.09$ at $+17$ days. The evolution in IR bands is slow, and only after day $+200$ the object starts to decline in the IR too. Between $+200$ and $+256$ days it fades by ~ 1 mag in the K -band. However, later epoch observations provided by (Goranskij et al. 2016) and follow-up with P200 and NOT, suggest a re-brightening of the object in IR bands.

The colour evolution between -29 and $+272$ d for M101-OT is shown in Figure 4. Coincident with the end of the first phase of the lightcurve, at ~ 70 days, the object becomes slightly bluer in B and g -bands. This period is associated with a decrease of the photospheric radius, shown in the lower panel of Figure 2. At approximately $+130$ days, at the time of the end of the second plateau, the colour evolution shows a second temporary (~ 20 days) enhancement of flux ratio for the blue bands. The last multi-band epoch ($+154$ days) shows that the object becomes increasingly red, i.e. $g - r = 1.9 \pm 0.4$, $g - z = 3.8 \pm 0.4$ and $V - K = 5.6 \pm 0.2$.

2.2. Optical Spectroscopy

We obtained spectra of M101-OT using a range of facilities. The log of the spectroscopic observations is given in Table 6. The data were reduced using IRAF and PYRAF standard routines. The wavelength calibration was done by fitting low-order polynomials to arc lamp spectra. Sky lines were used to check the accuracy of the calibration, which is within 1 Å. We calibrated the flux using spectro-hotometric standard stars and later on adjusted it using interpolated photometry for the same epoch as the spectra.

We assumed the heliocentric recessional velocity for M101 of 241 ± 2 km s $^{-1}$ (de Vaucouleurs et al. 1991). Figure 5 shows the spectral evolution of M101-OT. All spectra show a cool photospheric continuum, fitted by a black-body emission with temperatures $3000 - 3600$ K.

The blue part of the M101-OT spectrum is dominated by the absorption forest of Fe II (at around 5400 Å), Ti II(below 4700 Å) and Sc II lines. P-Cygni profiles are displayed by intermediate-mass elements. Ca II is identified with an expansion velocity of $v \simeq -356 \pm 9$ km s $^{-1}$ for the absorption component at $+2$ days, slowing to $v \simeq -283 \pm 2$ km s $^{-1}$ at $+22$ days, and $v \simeq 207 \pm 17$

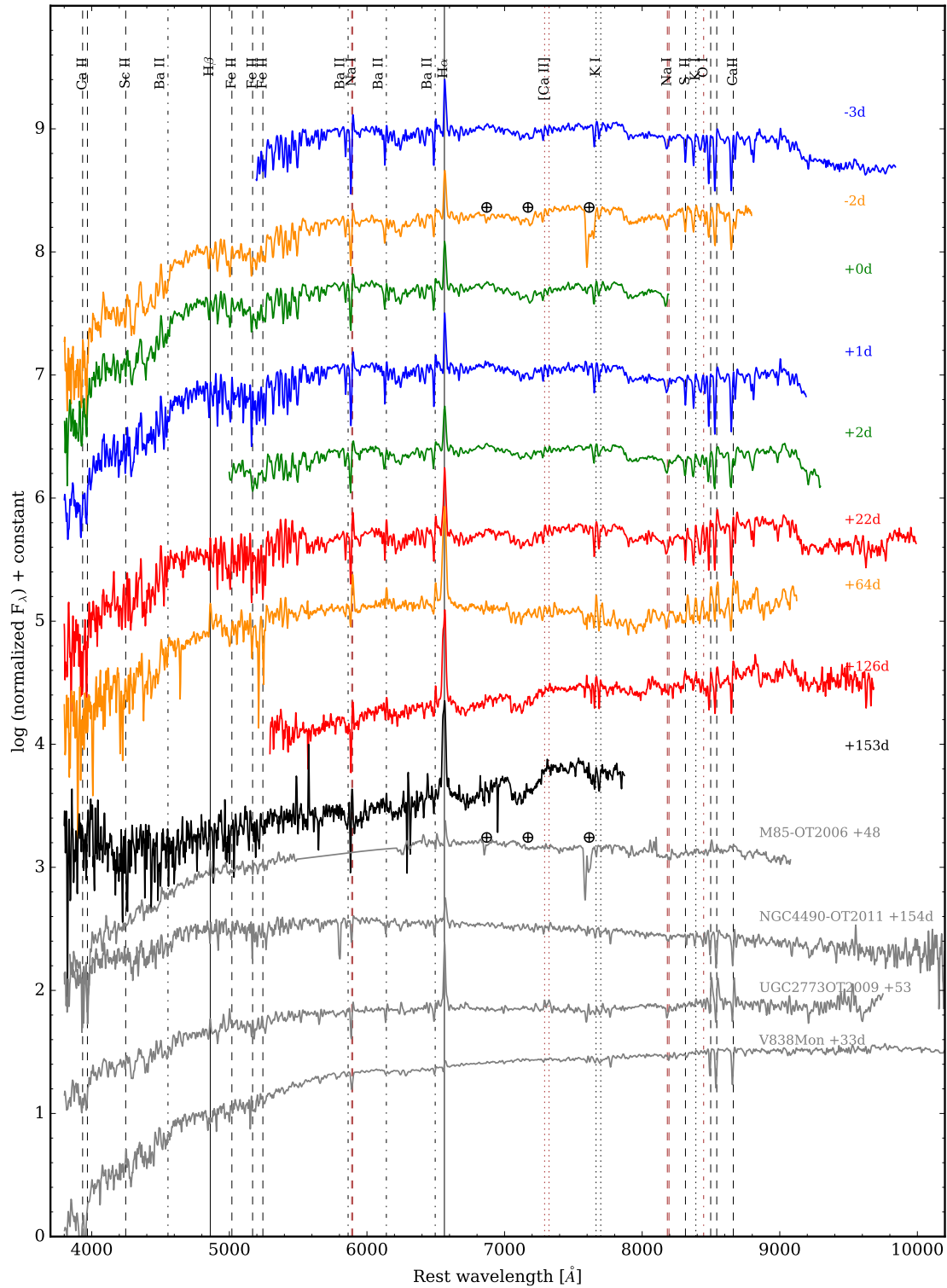


FIG. 5.— Spectral evolution of M101-OT. The spectra have been flux calibrated using the interpolated photometric measurements. Telluric absorption features were corrected or marked otherwise with \oplus symbol. Because the response of the detector drops at the extremes, some spectra are only shown for the valid wavelength range. The spectrum is colour coded by instrument. Blue: P200+DPSP, green: 1.82m+AFOSC, red: WHT+ISIS, orange: NOT+ALFOSC, black: GTC+OSIRIS, grey: comparison spectra.

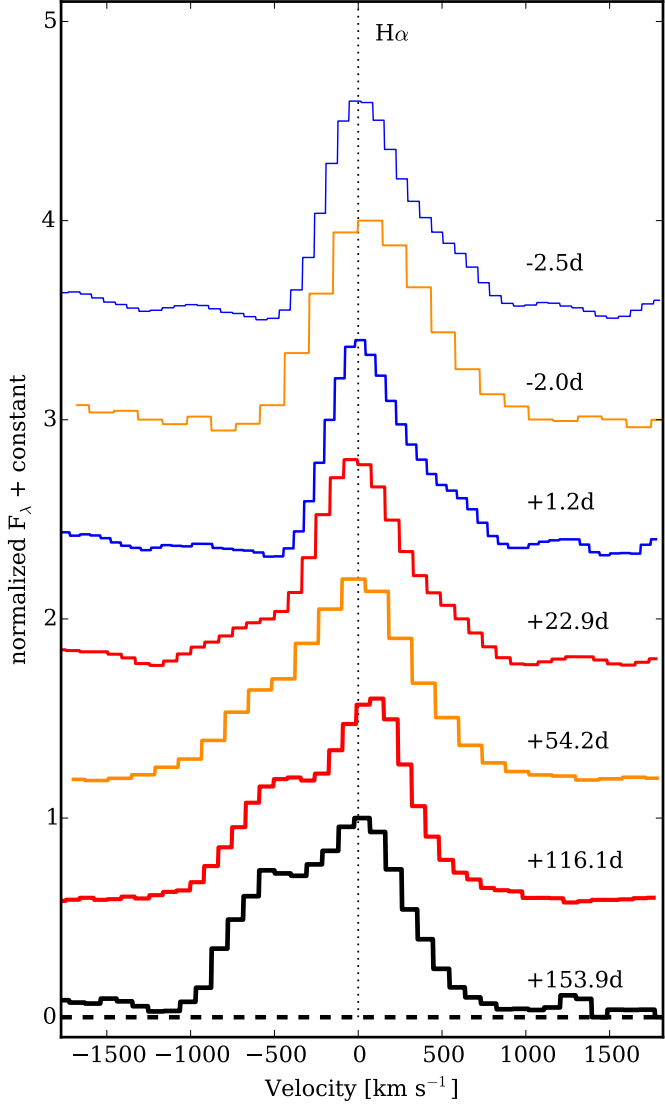


FIG. 6.— The continuum-subtracted and peak normalized H α region for DBSP (500 km s $^{-1}$), WHT (320 km s $^{-1}$), NOT (747 km s $^{-1}$) and GTC (380 km s $^{-1}$) spectra.

km s $^{-1}$ at +116 days. Ba II $\lambda\lambda$ 6134, 6489 is also identified as P-Cygni profile with an expansion velocity of -180 km s $^{-1}$ and a FWHM of 367 km s $^{-1}$. Other elements present in early-time spectra are $\lambda\lambda$ 5150 Mg $\lambda\lambda$ and Na I at $\lambda\lambda$ 5890, 5896 and $\lambda\lambda$ 8183, 8195. Resonance lines K I $\lambda\lambda$ 7665, 7699 and $\lambda\lambda$ 7665, 7699 are also found in the spectrum, although their P-Cygni profiles are much weaker. These lines are rare and have been seen in the extreme super-giant VY CMa (Smith 2004) and Type IIn SN 2009kn (Kankare et al. 2012). We do not detect strong [Ca II] $\lambda\lambda$ 7291, 7325 lines in the spectrum, which have been associated with dense and compact gas disk and presence of dust (Smith et al. 2010; Liermann et al. 2014). Figure 5 shows comparison spectra for similar red transients. M85-OT2006-1 is defined as an SN2008S-like observational class, showing strong emission for CaII and [Ca II] lines. UGC2773-OT2009-1 is considered to be an example of a dust enshrouded LBV. NGC4490-OT2011-1 and V838 Mon are examples

of LRNe. There is an important resemblance between all three groups, implying that the nature of the outburst can not be determined from spectra alone.

The spectra of M101-OT has a noticeable evolution of the H α profile. Figure 6 shows different morphologies of the profiles for different epochs. At early times, its expansion velocity, derived from the FWHM, is around 500 km s $^{-1}$, slightly larger than the one of intermediate mass elements. The profile is asymmetric and shows a small blueshifted absorption component. However, at +22.9 days the absorption evolves into an emission profile, suggesting the existence of asymmetry in the outflow. The implications of this are further discussed in Section 3.1.1. Similar behaviour was observed in the high resolution spectra of NGC4490-OT2011-1 reported in (Smith et al. 2016b).

3. ANALYSIS

3.1. Spectroscopic Analysis

3.1.1. The H α profile

An interesting feature is the evolution to a double peaked profile of the H α line (Fig. 6). There is evidence for a double peaked line, with a difference in velocity of ~ 500 km s $^{-1}$ between the components. Spectra taken around peak show the blueshifted P-Cygni component in absorption.

However, for later epochs, coincident with the beginning of the plateau phase at +17 days, the absorption disappears and an increasingly bright blueshifted emission peak appears instead. The second emission component becomes clearly visible at +54 days, and reaches similar equivalent width as the redshifted counterpart at +116 days.

Similar behaviour was also observed for likely merger events, such as LRNe V1309 Sco (Mason et al. 2010), NGC 4490 2011OT-1 (Smith et al. 2016b), which had higher spectral resolution data.

3.1.2. Molecular bands

Spectra taken at +116 days and later epochs show the initial formation of molecular bands, characteristic for cool M-type stars. Figure 7 shows the comparison between M101-OT spectrum at +154 days, with a cool M5III star and the Galactic merger V838 Mon, seven years after its outburst. At this phase, the photospheric temperature shows a good fit with ~ 3000 K black-body. We detect titanium oxide (TiO) bands in the range 6600-6800 Å and 7050-7300 Å. Between 7300 and 7600 Å, TiO absorption is combined with vanadium oxide (VO) molecular absorption, which becomes dominant above 7400 Å.

3.2. SED analysis and bolometric lightcurve

We computed a black-body fit to several pre- and post-discovery epochs, preferentially taken around the same epoch, or at most ± 50 days from each other. In the case that a particular band had more than one measurement within the time interval, we computed the mean value weighted by the errors.

We used the MCMC PYTHON package EMCEE (Foreman-Mackey et al. 2013) to obtain the value of the maximum posterior probability and 1σ confidence inter-

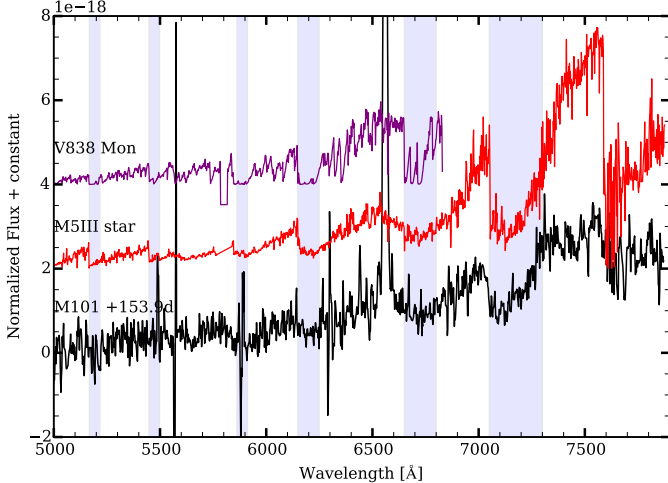


FIG. 7.— Comparison of M101-OT spectrum at +154 days with HD118767 M5III star and the average spectrum of V838 Mon (Tylenda et al. 2011). The spectrum has an estimated black-body temperature of ~ 3000 K. The molecular bands are comparable to the ones in cool giant stars. Major telluric absorption lines are marked in the spectrum with blue vertical bands.

vals on the estimated parameters. The evolution of temperature and radius for the best black-body fit is shown in the lower panels of Figure 2. In all cases, a single black-body component was sufficient to describe the observed spectral energy distribution.

The initial fits for the progenitor at epochs earlier than 6 years, show that the temperature and radius were constant within the errors with values of $T = 6600 \pm 300$ K and an $R = 220 \pm 13$ R_{\odot} . Starting at -5.5 years, there was a progressive expansion and cooling of the star, so that during outburst the temperature had decreased to roughly 3300 K, and continued to cool down slowly over the next 160 days. Along with the cooling process, the radius had grown exponentially up to $R \sim 7400$ R_{\odot} during outburst peak, receded to $R \sim 3600$ R_{\odot} at 70 days and expanded again to approximately $R \sim 8600$ R_{\odot} at 250 days. Similar behaviour was noticed for M31 2015 LRN (MacLeod et al. 2016). We fit a linear model for the radial expansion for epochs 60 to 152 days, which allowed to derive the photospheric expansion velocity of 115 ± 5 km s^{-1} .

The temperature at during the second peak is 3600 ± 100 K. There is a slow cooling, so that the photosphere cools until the object reaches 3000 K towards the end of the plateau phase, up to 120 days. IR photometry for later epochs show a much faster cooling rate. At +260 days, the temperature is consistent with 1200 K black-body emission.

The integrated black-body emission was used to estimate the bolometric lightcurve for M101-OT, shown in Figure 8. While the early time photometry shows a rather stable object with luminosity $L \simeq 2.6 \times 10^5$ L_{\odot} , photometry later than five years prior to the outburst shows a steady increase in the star's bolometric luminosity, reaching $L \sim 4 \times 10^5$ L_{\odot} at 250 days before and approximately $L \simeq 6.3 \times 10^6$ L_{\odot} during the maximum of the second outburst. This increase suggests an expansion of the stellar radius at an average rate of ~ 2.8 R_{\odot} year^{-1} (~ 22 km s^{-1}) during the pre-outburst phase.

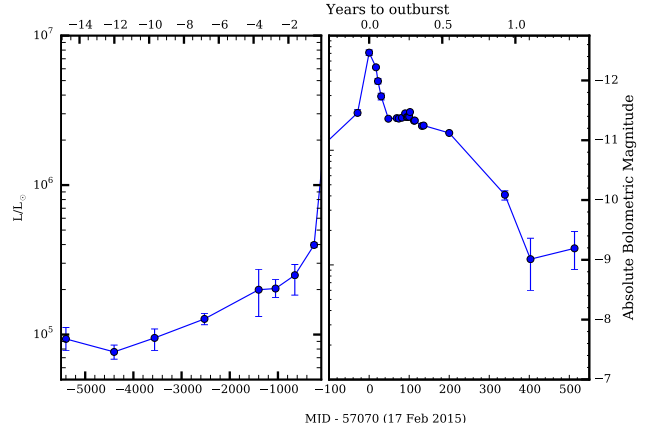


FIG. 8.— The evolution of the black-body luminosity of M101-OT. The last epochs were derived using NIR bands only.

3.3. Progenitor analysis

Photometric measurements from the earliest three archival epochs, obtained between 15 and 8 years before outburst, were used to derive the best parameters for the progenitor star. We found a good agreement with a single black-body fit. No significant IR excess was observed in the early photometric measurements. The star was estimated to have a temperature of $T = 6600 \pm 300$ K and an approximate radius of $R = 220 \pm 13$ R_{\odot} . The historic average bolometric luminosity is $L \sim 8.8 \pm 0.8 \times 10^4$ L_{\odot} , which placed the progenitor star to be below the low luminosity end of the LBV zone in the HR diagram (Smith 2004), where known LBVs tend to have luminosities greater than $L \sim 2 \times 10^5$ L_{\odot} .

In order to derive the characteristics of the progenitor system, we compared (using maximum likelihood) the observed photometric archival measurements with the predicted absolute magnitudes for single (Eldrige & Tout 2004) and for binary (Stanway et al. 2016) stellar evolution models with solar metallicity.

For the case of a single star evolution scenario, for a fixed Solar metallicity, the only free parameter of the model is the initial progenitor mass. The left hand side panel of Figure 9 shows the location of the progenitor star in the temperature-luminosity space for three historic measurements. The progenitor star is consistent with an F-type yellow super-giant, with initial mass of 18-19 M_{\odot} , that is evolving off the main sequence towards the red super-giant (RSG) phase. The location of the progenitor, named the Hertzsprung gap, is extremely unusual, as it is associated with stars that finished core hydrogen burning, but have not started yet the shell hydrogen burning phase. Stars are expected to spend only a small fraction of their lives (~ 3000 yr) in the region where the progenitor system is found, as shown in Figure 9.

For the case of a binary evolution scenario, the models have three free parameters: the initial mass of the binary system, the mass ratio and the initial period. We use the averaged photometric measurements over all epochs older than -5.5 years to compare with the predicted absolute magnitude of the models. We compute the maximum likelihood for all available models with masses in the $10 - 25$ M_{\odot} range, where the model parameter space is well sampled. The analysis shows that

the best fit model has initial masses $M1_{\text{ini}} = 18 \pm 1 M_{\odot}$ and $M2_{\text{ini}} = 16.2 \pm 0.9$ from the primary and secondary star respectively. The mass ratio is $q=0.9\pm0.1$, and the initial orbital period $P = \sim 400$ days. The initial separation of the model system was $724 R_{\odot}$ and the radius of the primary star, around $\sim 20 R_{\odot}$, so that they formed a detached binary system. The epoch with the maximum likelihood between the observed and the model is $\sim 9.89 \pm 0.01$ Myr, just 1 Myr after the primary star started to develop a He core. This time scale is coincident with major changes in the system. The primary, most evolved star, after initiating its expansion, reaches $\sim 200 R_{\odot}$, starting to overfill the Roche lobe with the secondary star and forming a CE. After the ejection of the envelope, occurring on dynamical timescales, the model predicts a surviving binary pair consisting in the He core of the primary star $M1 = 5 M_{\odot}$ and $M2 = 16.3$, which gains part of the mass transferred from the primary. The period of the system is expected to tighten to ~ 187 days after the interaction period. The estimated radius for the progenitor $R = 200 \pm 13 R_{\odot}$ matches with the transition phase when the primary radius overfills its Roche lobe, as shown in the right hand side panel of Figure 9. The pre-outburst photometry of the progenitor system fits well the characteristics of the system right at the moment of the Roche lobe overflow.

4. DISCUSSION

The absolute magnitude for M101-OT, $M_r^{\text{peak}} = -12.4$ mag, and its red colour, $g - r = 1.4$ mag during the secondary peak, places this event in the so-called “gap” region of the timescale-luminosity diagram between novae (-4 to -10 mag), and SNe (-15 to -22 mag). Photometrically, the double-peaked lightcurve of M101-OT and increasingly red colour resembles the complex nature of the objects in the LRNe group, with different scaling. However, such behaviour is also shown by objects interpreted as a SN impostor, such as SN Hunt 248, in NGC 5806 (Mauerhan et al. 2015; Kankare et al. 2015).

The lack of periodic microvariation in the lightcurve -15 to -5 years before outburst suggests that, unlike in the case of Galactic merger V1409 Sco, where both binary components were detected, for M101-OT only the brightest star in the system was seen. The unusual location of the progenitor in the Hertzsprung gap supports the hypothesis that star is quickly expanding after finishing the core H burning phase. If such star has a close companion, whenever it expands enough to overfill its Roche lobe, it will initiate the mass transfer towards the secondary, forming a Common Envelope (CE, see Ivanova et al. (2013) for a review) surrounding the binary system, so that the accretor will become engulfed in the envelope of the donor star.

Given the low densities in the outer layers of the donor atmosphere, the initial drag on the secondary may not be noticeable on short timescales. However, the spiral-in phase will accelerate with the secondary orbiting in increasingly denser layers of the primary star, eventually leading either to the merger of the components or the ejection of the envelope of the primary star on dynamical timescales. The slow brightening in M101-OT before the detected outbursts could have been associated with these final stages. The existence of optically thick ejected material is confirmed by the quick colour evolu-

tion of M101-OT in the blue bands, which suggests the existence optically thick ejected material.

The spectrum of M101-OT is dominated by H α , Ca II, Ba II, Na II and K I at low expansion velocities (~ 300 km s $^{-1}$) and a forest of Ti II and Fe II absorption lines at short wavelengths. These characteristics are similarly to other LRNe, such as V838 Mon, M31 LRN or NGC 4490 2011OT-1. However, low expansion velocities are not exclusive of this class. Members of LBVs and ILOT classes also show outflow velocities well below 1000 km s $^{-1}$. The double-peaked H α emission profile, tracing the bipolar structure of the ejecta, has also been observed in the asymmetric outflows of LBVs (Smith et al. 2016a) and nebular phases of SNe IIn with bipolar CSM (Smith et al. 2015; Andrews et al. 2016) or CCSNe, such as SN 1987A (Grönningsson et al. 2008). Newly formed dust within the ejecta is the responsible for the extinction of optical and NIR light. The redshifted component undergoes greater absorption from the generated dust, and therefore the blue emission may become more dominant at late epochs (Bevan & Barlow 2016).

One distinctive feature of M101-OT is the prompt formation of molecular bands, which suggest the presence of newly formed dust. At +154 days the spectrum showed evidence of formation of TiO and VO bands, comparable to the ones seen in LRNe V4332 Sgr (Martini et al. 1999; Kamiński et al. 2010) and V838 Mon Rushton et al. (2005); Tylenda et al. (2011). Figure 7 shows a comparison of the spectrum of M101-OT at +154 days, along with the UVES/VLT average spectrum of V838 Mon taken in January, February and March 2009, about seven years after the outburst (Tylenda et al. 2011). Although the resolution of the GTC spectrum is not high enough to resolve individual bands (380 km s $^{-1}$), they match well with a spectrum of an M5III star (Bagnulo et al. 2003).

Possible interpretations of the true nature of M101-OT may include a wide range of scenarios. Some examples are: mass-loss during turbulent phases of the stellar evolution (e.g. during the post He-burning phase); mass loss events triggered by the passage of a lower-mass companion to the periastron and the subsequent shell-shell collision in very eccentric orbits; a faint terminal explosion or event thermal emissions from shocks originated from the mass loss in the binary system (Pejcha et al. 2016). Goranskij et al. (2016)¹⁸ suggested the interpretation of M101-OT as a massive OB binary system.

We argue that, within the context of binary evolution models, M101-OT likely represents the best studied case on an unusual event of the ejection of the CE in a massive binary system, leaving two surviving components in a closer massive binary system formed by the lower mass main sequence star and the He core of the stripped companion.

5. SUMMARY AND CONCLUSIONS

M101-OT is a LRN discovered in a star formation region in a spiral arm of M101-OT. A summary of its most relevant observational characteristics is given below:

- The historic evolution of M101-OT shows no major

¹⁸ <http://www.vgoranskij.net/lrn2015-in-m101.pdf>

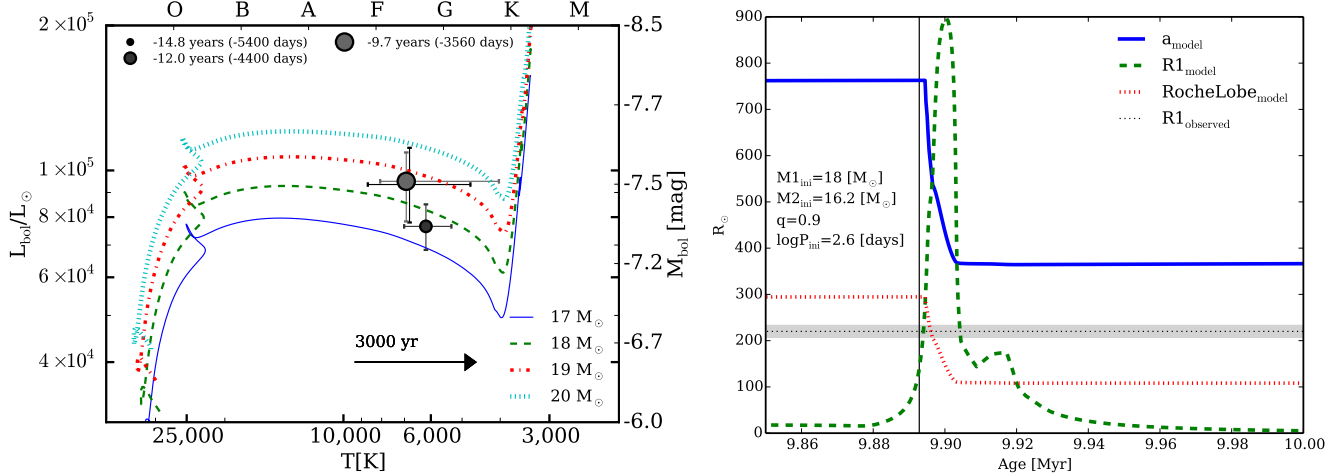


FIG. 9.— Left: The position of the progenitor of M101-OT for the first three initial epochs older than 2500 days, when L_{bol} is constant. The size of the point encodes the epoch of the observation relative to discovery. Stellar evolutionary tracks for single star models (Eldridge & Tout 2004) are shown for stars with initial masses from 17 to $20 M_{\odot}$. To provide a graphic example of the short live of stars in the progenitor region, the arrow shows the temperature evolution of a $18 M_{\odot}$ star in only 3000 years. Right: The maximum likelihood binary stellar model has $18 M_{\odot}$ as the mass of the primary, mass ratio $q = 0.9$ and initial period of 400 days. For this model, the Figure shows the evolution of a , the semi-major axis in R_{\odot} as blue solid line, the predicted radius of the primary star as red dotted line, the estimated radius of the Roche lobe for the primary star as green dashed line, the progenitor radius estimated from the observations is shown as a black dotted thin line. 1σ contours are marked with shaded areas. The vertical line shows the step with the maximum likelihood between the model and the photometry.

variations within 0.2 mag in R -band until approximately 5.5 years before the outburst.

- The object slowly brightens by 1.5 mags over the last 6 years before the outburst. The estimated radius appears to increase from $230 \pm 13 R_{\odot}$ at 6 years before the outburst, to $3100 R_{\odot}$ during the secondary outburst maximum.
- Black-body fits to pre-outburst optical, near and mid-IR photometry suggest the absence of an old existing dust emission component.
- The lightcurve shows two peaks, detected in R -band, separated by ≥ 100 days. The magnitude of the first peak is $M_r \geq -12.4$ mag (lower limit because of an observation gap) and $M_r = -12.0$ during the second peak. The colour of the object is $g - r = 1.4$ mag, which gives an estimated temperature of 3600 K.
- The bolometric luminosity for the second peak is $L = 2.7 \times 10^{33}$ ergs s^{-1} and the total energy release during the outburst is $L > 4.1 \times 10^{47}$ erg. This is only a lower limit, as the first outburst does not contain enough multi-band data to put a tight constraint on the energy.
- During peak, the spectrum shows a cold photospheric continuum, combined with low ejection velocities (~ 300 km s^{-1}) for $H\alpha$, Fe II and other low ionization elements, which display a P-Cygni profile.
- The lightcurve after the second outburst is defined by a short decline phase (~ 50 days), a “plateau” phase (~ 60 days) in riz bands and a second decline phase. Coincident with the first part of the lightcurve, the photosphere recedes to $3700 R_{\odot}$ at

+70 days, but restarts its expansion during the “plateau” phase. Late time follow-up photometry suggests the re-brightening of the object in IR wavelengths after one year.

- The $H\alpha$ line shows initially a blueshifted absorption component at -500 km s^{-1} , which develops into an emission profile at epochs +30 days or later.
- The spectrum shows the formation of molecular bands after 100 days of the outburst, which suggests the fast formation of dust in the system.
- Assuming a binary progenitor scenario, the best fit for the more massive component is an F-type giant with a luminosity of $L \sim 8.7 \times 10^4 L_{\odot}$. The system has a total mass of $\simeq 20 M_{\odot}$ and mass ratio $q \approx 0.9$. The estimated age of 9 Myr for the binary is qualitatively consistent with the young stellar population surrounding the progenitor, although high accuracy photometry will be needed to provide a quantitative answer.

Although the nature of the object is not entirely clear, its resemblance with other transients from the same LRN family points out a possible binary origin. The unusual location of the progenitor star in the Hertzsprung gap supports the hypothesis of the most massive component had expanded beyond initiating the CE phase. The outbursts in M101-OT suggest that these CE was ejected on dynamical timescales, leaving a surviving close binary pair.

We have discussed the past and present of this unusual transient in M101; discussion of its future and the fate of its progenitor will have to await further observations of its evolution in the IR bands.

ACKNOWLEDGMENTS

The research leading to these results has received funding from the European Union Seventh Framework Programme ([FP7/2007-2013] under grant agreement num.

264895. This work was partly supported by the European Union FP7 programme through ERC grant number 320360. This work was supported, in whole or in part, by the European Science Foundation under the GREAT ESF RNP programme. LANL participation in iPTF was funded by the US Department of Energy as part of the Laboratory Directed Research and Development program. Part of this research was carried out at the Jet Propulsion Laboratory, California Institute of Technology, under a contract with the National Aeronautics and Space Administration. Based on observations obtained with MegaPrime/MegaCam, a joint project of CFHT and CEA/IRFU, at the Canada-France-Hawaii Telescope (CFHT) which is operated by the National Research Council (NRC) of Canada, the Institut National des Sciences de l'Univers of the Centre National de la Recherche Scientifique (CNRS) of France, and the University of Hawaii. This work is based in part on data products produced at Terapix available at the Canadian Astronomy Data Centre as part of the Canada-France-Hawaii Telescope Legacy Survey, a collaborative project of NRC and CNRS. This paper makes use of data obtained from

the Isaac Newton Group Archive which is maintained as part of the CASU Astronomical Data Centre at the Institute of Astronomy, Cambridge. This work is partly based on observations obtained with the Nordic Optical Telescope, operated by the Nordic Optical Telescope Scientific Association at the Observatorio del Roque de los Muchachos, La Palma, Spain. This work is partly based on observations made with the William Herschel Telescope operated on the island of La Palma by the Isaac Newton Group in the Spanish Observatorio del Roque de los Muchachos of the Instituto de Astrofísica de Canarias. The Gran Telescopio Canarias (GTC) operated on the island of La Palma at the Spanish Observatorio del Roque de los Muchachos of the Instituto de Astrofísica de Canarias. This work is partly based on data from Copernico 1.82m telescope operated by INAF Osservatorio Astronomico di Padova. NER, AP, GT and MT are partially supported by the PRIN-INAF 2014 with the project “Transient Universe: unveiling new types of stellar explosions with PESSTO”. Finally, NBM would like to acknowledge Pablo and Lucia Solis and Israel Zenteno for providing the motivation in the last stages of this work.

APPENDIX

PHOTOMETRY TABLES

TABLE 1
HISTORIC PHOTOMETRIC MEASUREMENTS OF M101-OT.

Phase (days)	JD (+245000)	Tel.	m_U (mag)	m_B (mag)	m_V (mag)	m_R (mag)	m_u (mag)	m_g (mag)	m_r (mag)	m_i (mag)	m_z (mag)	m_y (mag)	Unfilt. (mag)	Refs.
-5413.5	1656.5	CFHT	-	21.94 \pm 0.11	21.89 \pm 0.31	21.16 \pm 0.19	-	-	-	-	-	-	-	-
-5410.8	1659.2	INT	-	-	-	-	-	-	21.17 \pm 0.17	-	-	-	-	-
-4364.0	2706.0	SDSS	-	-	-	-	23.13 \pm 0.49	21.79 \pm 0.09	21.86 \pm 0.14	21.31 \pm 0.08	21.94 \pm 0.58	-	-	[1]
-3920.1	3149.9	INT	-	21.83 \pm 0.22	-	-	-	-	-	-	-	-	-	-
-3860.6	3209.4	CFHT	-	-	-	-	21.82 \pm 0.36	21.38 \pm 0.13	-	-	-	-	-	-
...

6

NOTE. — References: [1], Kelly et al. (2015). Table 1 is published in its entirety in the machine-readable format. A portion is shown here for guidance regarding its form and content.

TABLE 2
POST-DISCOVERY PHOTOMETRIC MEASUREMENTS OF M101-OT.

Phase (days)	JD (+245000)	Tel.	m_U (mag)	m_B (mag)	m_V (mag)	m_R (mag)	m_I (mag)	m_u (mag)	m_g (mag)	m_r (mag)	m_i (mag)	m_z (mag)	Refs.
4.0	7074.0	SAI-2.5m	-	19.09 \pm 0.02	17.71 \pm 0.02	16.83 \pm 0.02	-	-	-	-	-	-	[1]
7.9	7077.9	SAO-6m	-	19.04 \pm 0.02	17.69 \pm 0.02	16.83 \pm 0.02	-	-	-	-	-	-	[1]
11.1	7081.1	SAI-2.5m	-	19.23 \pm 0.02	17.79 \pm 0.02	16.90 \pm 0.02	-	-	-	-	-	-	[1]
17.1	7087.1	NOT	-	19.57 \pm 0.05	18.12 \pm 0.02	17.07 \pm 0.01	16.35 \pm 0.05	-	-	-	-	-	-
22.2	7092.2	LT	-	19.90 \pm 0.26	-	-	-	-	19.06 \pm 0.20	17.73 \pm 0.06	17.23 \pm 0.08	16.88 \pm 0.07	-
...

NOTE. — References: [1] Goranskij et al. (2015). Table 2 is published in its entirety in the machine-readable format. A portion is shown here for guidance regarding its form and content.

TABLE 3
PTF FOLLOW-UP DATA OF M101-OT.

Phase (days)	JD (+245000)	Telescope	m_g (mag)	m_r (mag)	m_i (mag)
-2005.8	5064.2	PTFP48	-	20.26 \pm 0.11	-
-1706.7	5363.3	PTFP48	-	20.31 \pm 0.11	-
-1682.7	5387.3	PTFP48	-	20.18 \pm 0.15	-
-1484.6	5585.4	PTFP48	-	20.17 \pm 0.13	-
-1345.7	5724.3	PTFP48	-	20.25 \pm 0.14	-
...

NOTE. — The errors are given in brackets. Table 3 is published in its entirety in the machine-readable format. A portion is shown here for guidance regarding its form and content.

TABLE 4
NIR AND MIR PHOTOMETRY OF M101-OT.

Phase (days)	JD (+245000)	Telescope	<i>J</i> (mag)	<i>H</i> (mag)	<i>K</i> (mag)	$3.6\mu\text{m}$ (mag)	$4.5\mu\text{m}$ (mag)
-4065.0	3005.0	Spitzer	—	—	—	19.00 ± 0.01	18.60 ± 0.01
-3997.5	3072.5	Spitzer	—	—	—	—	>20.48
-2075.0	4995.0	CFHT	22.74 ± 0.53	—	19.54 ± 0.11	—	—
-1756.6	5313.4	UKIRT	20.61 ± 0.16	—	—	—	—
17.1	7087.1	NOT	15.48 ± 0.03	15.10 ± 0.06	14.97 ± 0.09	—	—
48.0	7118.0	NOT	16.42 ± 0.03	15.74 ± 0.05	15.47 ± 0.01	—	—
62.6	7132.6	Spitzer	—	—	—	14.72 ± 0.01	14.75 ± 0.01
74.0	7144.0	NOT	16.70 ± 0.04	15.72 ± 0.02	15.49 ± 0.07	—	—
90.3	7160.3	Spitzer	—	—	—	14.55 ± 0.01	14.59 ± 0.01
102.0	7172.0	NOT	16.63 ± 0.03	15.90 ± 0.04	15.41 ± 0.06	—	—
121.8	7191.8	Spitzer	—	—	—	14.50 ± 0.01	—
136.0	7206.0	NOT	16.53 ± 0.02	16.01 ± 0.03	15.46 ± 0.04	—	—
150.8	7220.8	Spitzer	—	—	—	14.39 ± 0.01	—
197.9	7267.9	NOT	17.16 ± 0.03	16.02 ± 0.03	15.25 ± 0.02	—	—
202.7	7272.7	Spitzer	—	—	—	14.30 ± 0.01	14.50 ± 0.01
253.3	7323.3	NOT	—	17.87 ± 0.07	16.32 ± 0.03	—	—
280.3	7350.3	NOT	—	>16.56	16.81 ± 0.07	—	—
339.0	7409.0	SAI-2.5m	18.65 ± 0.05	17.64 ± 0.10	16.32 ± 0.05	—	—
385.0	7455.0	SAI-2.5m	21.00 ± 0.20	20.20 ± 0.30	18.20 ± 0.20	—	—
403.4	7473.4	P200	21.85 ± 0.42	19.59 ± 0.17	17.91 ± 0.12	—	—
438.0	7508.0	NOT	—	—	17.22 ± 0.12	—	—
514.0	7584.0	NOT	20.01 ± 0.24	18.77 ± 0.13	17.25 ± 0.13	—	—

TABLE 5
SEQUENCE STAR MAGNITUDES USED FOR THE M101 FIELD. THE VALUES ARE COMPUTED FROM THE STACKED MAGNITUDES FROM PAN-STARRS.

Star #	α (J2000.0)	δ (J2000.0)	m_g (mag)	m_r (mag)	m_i (mag)	m_z (mag)	m_y
1	210.6328	54.4887	18.347 (0.007)	17.488 (0.004)	17.123 (0.004)	16.935 (0.006)	16.836 (0.007)
2	210.5005	54.4851	17.463 (0.005)	16.388 (0.005)	15.776 (0.004)	15.498 (0.004)	15.357 (0.004)
3	210.6519	54.4464	16.426 (0.004)	15.692 (0.004)	15.398 (0.004)	15.277 (0.004)	15.190 (0.005)
4	210.6370	54.4479	16.863 (0.006)	15.915 (0.005)	15.534 (0.005)	15.359 (0.003)	15.251 (0.006)
5	210.5874	54.4614	17.171 (0.007)	16.394 (0.005)	16.097 (0.005)	15.954 (0.003)	15.872 (0.005)
6	210.5708	54.4583	17.300 (0.007)	16.263 (0.004)	15.806 (0.004)	15.580 (0.004)	15.457 (0.005)
7	210.5798	54.4493	15.396 (0.005)	14.510 (0.004)	14.128 (0.004)	13.940 (0.003)	13.830 (0.004)
8	210.6340	54.4175	19.256 (0.012)	18.031 (0.006)	17.273 (0.004)	16.915 (0.005)	16.745 (0.008)
9	210.6171	54.4159	17.990 (0.011)	16.725 (0.004)	15.850 (0.005)	15.444 (0.003)	15.242 (0.005)
10	210.6189	54.4048	16.238 (0.004)	15.794 (0.003)	15.631 (0.003)	15.577 (0.003)	15.547 (0.005)
11	210.4896	54.4296	16.789 (0.011)	16.347 (0.004)	16.250 (0.004)	16.183 (0.004)	16.172 (0.007)
12	210.5186	54.4001	18.317 (0.007)	17.516 (0.004)	17.191 (0.005)	17.012 (0.006)	16.901 (0.007)
13	210.5614	54.4480	21.791 (0.110)	21.516 (0.062)	21.341 (0.060)	20.938 (0.205)	nan (nan)
14	210.5582	54.4429	19.752 (0.022)	19.292 (0.010)	19.133 (0.010)	19.080 (0.017)	18.984 (0.039)
15	210.5892	54.4280	19.388 (0.012)	18.499 (0.007)	18.187 (0.005)	18.024 (0.008)	17.918 (0.018)
16	210.5873	54.4296	22.027 (0.185)	21.018 (0.051)	19.627 (0.013)	19.041 (0.018)	18.646 (0.028)
17	210.5272	54.4393	21.070 (0.036)	20.555 (0.028)	20.313 (0.022)	20.209 (0.041)	19.641 (0.107)
18	210.5204	54.4523	21.392 (0.048)	21.017 (0.039)	20.799 (0.034)	20.758 (0.072)	nan (nan)
19	210.4864	54.4320	19.935 (0.017)	18.712 (0.007)	17.673 (0.004)	17.199 (0.005)	16.962 (0.010)

The errors are given in brackets. Coordinates and magnitudes are taken from the Pan-STARRS PV2 Catalog.

TABLE 6
LOG OF SPECTROSCOPIC OBSERVATIONS OF M101-OT.

Phase ^a	JD (d)	Date (245000+)	Telescope+Instrument	Grating/Grism	Dispersion (Å/pix)	Resolution ^b (km/s)	Exposure (s)
-2.5	7067.5	2015 Feb 14.5	P200+DBSP	7500	1.52	500	900
-2.0	7068.0	2015 Feb 15	NOT+ALFOSC	Grism#4	3.0	733	1800
0.1	7070.1	2015 Feb 17.1	Copernico 1.82m+AFOSC	GR04	4.7	630	1800
1.5	7071.5	2015 Feb 18.5	P200+DBSP	158/7500	1.52	420	1800
2.1	7072.1	2015 Feb 19.0	Copernico 1.82m+AFOSC	GR04	5.2	690	1800
22.9	7092.9	2015 Mar 11.9	WHT+ISIS	R300B+R158R	0.86+1.8	320	$2\times 600+2\times 600$
54.2	7124.2	2015 Apr 13.2	NOT+ALFOSC	Grism#4	3.0	747	2700
116.1	7186.1	2015 Jun 13.3	WHT+ISIS	R158R	1.8	345	2×1800
153.9	7223.9	2015 Jul 20.9	GTC+OSIRIS	R1000B	2.1	380	2×1800.0

^a Days since second peak at MJD 57070. ^b Measured using the FWHM of λ 5577 O I sky line.

REFERENCES

Adams, S. M., & Kochanek, C. S. 2015, MNRAS, 452, 2195

Ahn, C. P., Alexandroff, R., Allende Prieto, C., et al. 2014, ApJS, 211, 17

Andrews, J. E., Krafton, K. M., Clayton, G. C., et al. 2016, MNRAS, 457, 3241

Bagnulo, S., Jehin, E., Ledoux, C., et al. 2003, The Messenger, 114, 10

Bevan, A., & Barlow, M. J. 2016, MNRAS, 456, 1269

Bond, H. E., Bedin, L. R., Bonanos, A. Z., et al. 2009, ApJ, 695, L154

Bond, H. E., Henden, A., Levay, Z. G., et al. 2003, Nature, 422, 405

Botticella, M. T., Pastorello, A., Smartt, S. J., et al. 2009, MNRAS, 398, 1041

Cao, Y., Kasliwal, M. M., Chen, G., & Arcavi, I. 2015, The Astronomer's Telegram, 7070, 1

Cenko, S. B., Fox, D. B., Moon, D.-S., et al. 2006, PASP, 118, 1396

de Vaucouleurs, G., de Vaucouleurs, A., Corwin, Jr., H. G., et al. 1991, S&T, 82, 621

Eldridge, J. J., & Tout, C. A. 2004, MNRAS, 353, 87

Fazio, G. G., Hora, J. L., Allen, L. E., et al. 2004, ApJS, 154, 10

Foley, R. J., Berger, E., Fox, O., et al. 2011, ApJ, 732, 32

Foreman-Mackey, D., Hogg, D. W., Lang, D., & Goodman, J. 2013, Publications of the Astronomical Society of the Pacific, 125, 306

Fraser, M., Inserra, C., Jerkstrand, A., et al. 2013, MNRAS, 433, 1312

Gerke, J., Adams, S. M., Kochanek, C. S., & Stanek, K. Z. 2015, The Astronomer's Telegram, 7069, 1

Goranski, V. P., Cherjasov, D. V., Safonov, B. S., et al. 2015, The Astronomer's Telegram, 7206, 1

Goranski, V. P., Tatarenko, A. M., Shatsky, N. I., et al. 2016, The Astronomer's Telegram, 8599

Grönningsson, P., Fransson, C., Lundqvist, P., et al. 2008, A&A, 479, 761

Gwyn, S. D. J. 2008, PASP, 120, 212

Humphreys, R. M., & Davidson, K. 1994, PASP, 106, 1025

Iben, Jr., I., & Tutukov, A. V. 1992, ApJ, 389, 369

Ivanova, N., Justham, S., Chen, X., et al. 2013, A&A Rev., 21, 59

Kamiński, T., Schmidt, M., & Tylenda, R. 2010, A&A, 522, A75

Kankare, E., Ergon, M., Bufano, F., et al. 2012, MNRAS, 424, 855

Kankare, E., Kotak, R., Pastorello, A., et al. 2015, A&A, 581, L4

Kasliwal, M. M. 2011, Bulletin of the Astronomical Society of India, 39, 375

Kasliwal, M. M., Kulkarni, S. R., Arcavi, I., et al. 2011, ApJ, 730, 134

Kelly, P., Van Dyk, S., Fox, O., Filippenko, A. V., & Foley, R. 2015, The Astronomer's Telegram, 7082, 1

Khan, R., Stanek, K. Z., Prieto, J. L., et al. 2010, ApJ, 715, 1094

Kochanek, C. S. 2011, ApJ, 741, 37

Kulkarni, S. R., Ofek, E. O., Rau, A., et al. 2007, Nature, 447, 458

Liermann, A., Schnurr, O., Kraus, M., et al. 2014, MNRAS, 443, 947

MacLeod, M., Macias, P., Ramirez-Ruiz, E., et al. 2016, ArXiv e-prints, arXiv:1605.01493

Magnier, E. A., Schlaflly, E., Finkbeiner, D., et al. 2013, ApJS, 205, 20

Martini, P., Wagner, R. M., Tomaney, A., et al. 1999, AJ, 118, 1034

Masci, F. J., Hoffman, D. I., Grillmair, C. J., & Cutri, R. M. 2014, AJ, 148, 21

Mason, E., Diaz, M., Williams, R. E., Preston, G., & Bensby, T. 2010, A&A, 516, A108

Mauerhan, J. C., Smith, N., Filippenko, A. V., et al. 2013, MNRAS, 430, 1801

Mauerhan, J. C., Van Dyk, S. D., Graham, M. L., et al. 2015, MNRAS, 447, 1922

Nandez, J. L. A., Ivanova, N., & Lombardi, Jr., J. C. 2014, ApJ, 786, 39

Nugent, P. E., Sullivan, M., Cenko, S. B., et al. 2011, Nature, 480, 344

Ofek, E. O., Kulkarni, S. R., Rau, A., et al. 2008, ApJ, 674, 447

Ofek, E. O., Laher, R., Law, N., et al. 2012, PASP, 124, 62

Pastorello, A., Della Valle, M., Smartt, S. J., et al. 2007, Nature, 449, 1

Pastorello, A., Cappellaro, E., Inserra, C., et al. 2013, ApJ, 767, 1

Pejcha, O., Metzger, B. D., & Tomida, K. 2016, MNRAS, 455, 4351

Perryman, M. A. C., de Boer, K. S., Gilmore, G., et al. 2001, A&A, 369, 339

Prieto, J. L., Sellgren, K., Thompson, T. A., & Kochanek, C. S. 2009, ApJ, 705, 1425

Prieto, J. L., Kistler, M. D., Thompson, T. A., et al. 2008, ApJ, 681, L9

Rau, A., Ofek, E. O., Kulkarni, S. R., et al. 2008, ApJ, 682, 1205

Rich, R. M., Mould, J., Picard, A., Frogel, J. A., & Davies, R. 1989, ApJ, 341, L51

Rushton, M. T., Geballe, T. R., Filippenko, A. V., et al. 2005, MNRAS, 360, 1281

Schlaflly, E. F., & Finkbeiner, D. P. 2011, ApJ, 737, 103

Schlaflly, E. F., Finkbeiner, D. P., Jurić, M., et al. 2012, ApJ, 756, 158

Shappee, B. J., & Stanek, K. Z. 2011, ApJ, 733, 124

Smith, N. 2004, MNRAS, 349, L31

Smith, N., Andrews, J. E., Mauerhan, J. C., et al. 2016a, MNRAS, 455, 3546

Smith, N., Li, W., Silverman, J. M., Ganeshalingam, M., & Filippenko, A. V. 2011, MNRAS, 415, 773

Smith, N., Miller, A., Li, W., et al. 2010, AJ, 139, 1451

Smith, N., Mauerhan, J. C., Cenko, S. B., et al. 2015, MNRAS, 449, 1876

Smith, N., Andrews, J. E., Van Dyk, S. D., et al. 2016b, MNRAS, 458, 950

Sparks, W. B., Bond, H. E., Cracraft, M., et al. 2008, AJ, 135, 605

Stanway, E. R., Eldridge, J. J., & Becker, G. D. 2016, MNRAS, 456, 485

Thompson, T. A., Prieto, J. L., Stanek, K. Z., et al. 2009, ApJ, 705, 1364

Tonry, J. L., Stubbs, C. W., Lykke, K. R., et al. 2012, ApJ, 750, 99

Tylenda, R., Hajduk, M., Kamiński, T., et al. 2011, A&A, 528, A114

Tylenda, R., Kamiński, T., Udalski, A., et al. 2013, A&A, 555, A16

Walborn, N. R., Stahl, O., Gamen, R. C., et al. 2008, ApJ, 683, L33

Williams, S. C., Darnley, M. J., Bode, M. F., & Steele, I. A. 2015, ApJ, 805, L18

Wolf, B. 1989, in Astrophysics and Space Science Library, Vol. 157, IAU Colloq. 113: Physics of Luminous Blue Variables, ed. K. Davidson, A. F. J. Moffat, & H. J. G. L. M. Lamers, 91–98